Many-body localization with synthetic gauge fields in disordered Hubbard chains

Kuldeep Suthar [1,*] Piotr Sierant [1,2,†] and Jakub Zakrzewski [1,3,‡]

[1] *Institute of Theoretical Physics, Jagiellonian University in Krakow, Łojasiewicza 11, 30-348 Kraków, Poland*

[2] *ICFO—Institut de Sciences Fotoniques, The Barcelona Institute of Science and Technology, 08860 Castelldefels, Barcelona, Spain*

[3] *Mark Kac Complex Systems Research Center, Jagiellonian University in Krakow, Łojasiewicza 11, 30-348 Kraków, Poland*

(Received 30 January 2020; revised manuscript received 2 April 2020; accepted 13 April 2020; published 30 April 2020)

We analyze the localization properties of the disordered Hubbard model in the presence of a synthetic magnetic field. An analysis of level spacing ratios shows a clear transition from ergodic to many-body localized phase. The transition shifts to larger disorder strengths with increasing magnetic flux. Study of dynamics of local correlations and entanglement entropy indicates that charge excitations remain localized whereas spin degree of freedom gets delocalized in the presence of the synthetic flux. This residual ergodicity is enhanced by the presence of the magnetic field with dynamical observables suggesting incomplete localization at large disorder strengths. Furthermore, we examine the effect of quantum statistics on the local correlations and show that the long-time spin oscillations of a hard-core boson system are destroyed as opposed to the fermionic case.

DOI: 10.1103/PhysRevB.101.134203

I. INTRODUCTION

The phenomenon of many-body localization (MBL) has attracted a significant interest in condensed matter physics over the past several years, both theoretically [1–4] and experimentally [5–8]. The MBL is an extension of Anderson localization (which describes localization of single-particle eigenstates in the presence of disorder potential) to highly excited eigenstates of interacting many-body systems. The characteristic properties of a MBL phase are Poisson eigenvalue statistics [9–15], an absence of thermalization [16–19], a vanishing transport [20–22], and the logarithmic spreading of the entanglement entropy [23–25]. Starting from early works, many aspects of the topic have been examined to date. Ultracold atomic systems are an ideal platform to explore the localization phenomena due to their ability to tune dimensionality, nature of applied disorder, atomic interactions, lattice geometry, and synthetic gauge fields. The existence of a MBL phase has been confirmed in recent quantum gas experiments using quantum simulators such as optical lattices [5,6,26,27] and trapped ions [7].

The nonergodic behavior of a disordered Hubbard chain at strong disorder and temporal evolution of its correlation functions have been examined theoretically in Refs. [25,28]. The SU(2) symmetry of the model limits the full MBL as the charge degrees of freedom are localized but spins remain delocalized and reveal subdiffusive dynamics [29–31]. The partial MBL is due to the separation of timescales between charge and spin sectors dynamics in the presence of spin-independent disorder [32]. It was also suggested that transport properties strongly depend on the fraction of singly occupied sites in the initial state [33]. Still, the breaking of SU(2) spin symmetry recovers the full MBL phase [31,34,35]. The experimental study of a related cold atomic system [5,27] mainly addressed the charge sector observing signatures of MBL for available experimentally times of about 100 characteristic tunneling times in the optical lattice.

Most of the disorder-related studies consider time-reversal-invariant (TRI) Hamiltonians. Only very recently, experimental studies in cold atomic systems utilizing synthetic gauge fields addressed aspects of single particle localization. The work [36] studied the significance of symmetry on the localization and transport properties in the presence of synthetic gauge field for a periodically driven (Floquet) system while Ref. [37] exploited a lattice in the momentum space with laser-induced couplings to create a zigzag chain with the synthetic flux-dependent mobility edge. Single particle localization with synthetic random flux in a lattice has been discussed in Refs. [38,39]. Cheng and Mondaini [38] also studied the model with interaction, observing that the presence of random synthetic fluxes delocalized the system. The interacting fermion model Hamiltonian projected on a single Landau level in the presence of disorder [40] revealed signatures of MBL in the presence of magnetic flux but the effects observed were very strongly dependent on the system size. That led the authors to postulate the absence of localization in their model in the thermodynamic limit. Apart from these two studies, we are not aware of any studies of TRI symmetry breaking effects in the presence of disorder for interacting systems. The aim of the present paper is to partially fill this gap, considering experimentally accessible model on a lattice with diagonal disorder.

In particular, we examine the spectral and dynamical properties of disordered Hubbard chains in the presence of synthetic gauge fields. At lower disorder strengths, in the ergodic regime, the TRI symmetry breaking by gauge field results in spectral statistics well described by Gaussian orthogonal en-

*kuldeep.suthar@uj.edu.pl
†piotr.sierant@uj.edu.pl
‡jakub.zakrzewski@uj.edu.pl

semble (GOE) of random matrices instead of Gaussian unitary ensemble (GUE) as expected for broken TRI. This is due to a residual discrete symmetry. Only when the residual reflection symmetry is broken by local field or asymmetric tunneling rate of spin-up and spin-down fermions, the level statistics is characterized by GUE. While the time dynamics of charge and spin correlations for random initial states for the TRI case reveal the localization of charges and a subdiffusive decay of spin correlations [29–32], the introduction of a synthetic flux damps the spin oscillations and delocalizes the spins. Furthermore, the entanglement entropy confirms the delocalization of spins in the presence of the synthetic gauge fields.

The paper is organized as follows. In Sec. II, we introduce the Hubbard model with synthetic gauge field and disorder. In Sec. III, we analyze the effect of symmetry breaking and synthetic flux on the spectral properties of the system. We further study the local charge and spin dynamics of fermions and hard-core bosons in Sec. IV. In Sec. V, we examine the bipartite entanglement entropy. The local correlations in the presence of spin-dependent disorder are discussed in Sec.VI, followed by remarks on participation ratio of eigenvectors in Sec. VII. Finally, we conclude in Sec. VIII.

II. THE MODEL

We consider interacting spin-1/2 fermions in a quasi-one-dimensional lattice. The two spin components can be interpreted as the realization of a two-leg ladder geometry, with two legs corresponding to two spin states. Two components may be realized as in the recent experiment [5] for ^{40}K atoms with spin-up state being $|F, m_F\rangle = |\frac{9}{2}, -\frac{7}{2}\rangle \equiv |\uparrow\rangle$ and the spin-down state $|\frac{9}{2}, -\frac{9}{2}\rangle \equiv |\downarrow\rangle$. The two spin components may be coupled by, e.g., Raman coupling realizing the Hamiltonian [41,42] $\hat{H} = \hat{H}_0 + \hat{H}_{\rm sb}$, wherein

$$\begin{aligned}\hat{H}_0 = \hat{H}_H + \hat{H}_K = &-\sum_{j,\sigma}(J_\sigma\, \hat{c}^\dagger_{j,\sigma}\hat{c}_{j+1,\sigma} + \text{H.c.})\\ &+U\sum_j \hat{n}_{j,\uparrow}\hat{n}_{j,\downarrow} + \sum_{j,\sigma}\epsilon_j\hat{n}_{j,\sigma}\\ &-K\sum_j(e^{-i\gamma j}\hat{c}^\dagger_{j,\uparrow}\hat{c}_{j,\downarrow} + \text{H.c.}).\end{aligned} \tag{1}$$

Here, j and $\sigma = \uparrow, \downarrow$ are the spatial and spin indices, J_σ is the hopping amplitude between neighboring lattice sites on the same leg, σ, $\hat{c}^\dagger_{j,\sigma}(\hat{c}_{j,\sigma})$ creates (annihilates) fermions with spin σ at site j, and the occupation number operator is $\hat{n}_{j,\sigma} = \hat{c}^\dagger_{j,\sigma}\hat{c}_{j,\sigma}$. The local "charge" density is $n_j = n_{j,\uparrow} + n_{j,\downarrow}$ while the spin magnetization is $m_j = n_{j,\uparrow} - n_{j,\downarrow}$. The on-site interaction strength of two spins is assumed to be repulsive, i.e., $U > 0$ and ϵ_j is the uniform distribution of a random spin-independent on-site potential, $\epsilon_j \in [-W/2, W/2]$ with W being the disorder amplitude. All these parameters contribute to the standard Hubbard part of the Hamiltonian, H_H. Note that we allow, in principle, for spin-dependent tunneling rates, J_σ. Unless explicitly stated, we assume, however, that $J_\uparrow = J_\downarrow = J$, recovering the standard disordered Hubbard model. The second part of the Hamiltonian Eq. (1), H_K, couples two legs of the ladder with K being the amplitude and γ contributing to phase γj of the complex hopping in the synthetic dimension. γ represents the synthetic magnetic flux per plaquette of the lattice. In a laser-induced tunneling scheme (see, e.g., Ref. [42]), $\gamma = 2k_R a$ where k_R is the recoil wave vector of the laser and a is the lattice spacing. The finite value of γ leads to complex hoppings along the rungs of the ladder (corresponding to flipping the spins). Along the synthetic dimension, the system consists of two sites; this might be changed by trapping species in additional Zeeman components, e.g., $|F, m_F\rangle = |\frac{9}{2}, -\frac{5}{2}\rangle$. We restrict ourselves to the case already realized in experiments [5]. The gauge is chosen in such a way that the Peierls phase is along the rungs and not on the legs of the ladder—compare Fig. 1. The above model Hamiltonian without a synthetic gauge field has been realized in quantum gas experiments in optical lattices [5]; similarly, physics with the synthetic dimension in clean, disorder-free experiments has also been studied [43].

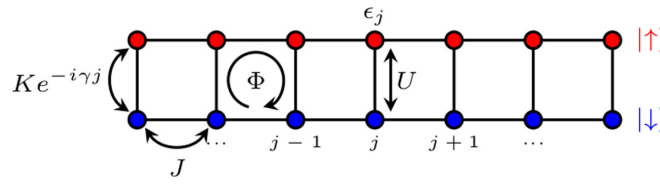

FIG. 1. Schematic visualization of the system studied Eq. (1) in which up (down)-spin corresponds to upper (lower) leg of the ladder. The magnetic flux per plaquette $\Phi = \gamma/2\pi$ [41].

The hopping amplitude sets the unit of energy scale, $J = 1$, and we use periodic boundary conditions throughout this paper. We study the system at unit filling (the total number of fermions $N = N_\uparrow + N_\downarrow = L$ is conserved and equal to a number of sites along the ladder). Note that such a situation is sometimes called a half filling in condensed-matter community.

The system concerned has a number of symmetries that have to be taken into account. In the absence of the gauge field ($K = 0$), the model Hamiltonian preserves parity (i.e., the exchange between up- and down-oriented spins), time-reversal and SU(2) spin symmetry [44], however, pseudospin SU(2) [45] and particle-hole symmetries are broken due to the on-site disorder potential. The parity and SU(2) spin symmetry can be removed by adding a local weak magnetic field (h_b) at the edge of the chain [25]. The symmetry-breaking Hamiltonian is

$$\hat{H}_{\rm sb} = h_b(\hat{n}_{1,\uparrow} - \hat{n}_{1,\downarrow}). \tag{2}$$

An alternative approach to obtain the same effect is to allow different tunneling rates for down-spin fermions $J_\downarrow = J$ and for up-spin fermions $J_\uparrow = J + \Delta J$. Such a realization may be simpler in cold atom implementation of the model (it is enough to go away from the so-called magic wavelength for lasers forming the optical lattice [5]) than creating a local magnetic field. In the absence of H_K that induces coupling between the legs of the ladder, the number of up-spin, $N_\uparrow$, and that of down-spin, $N_\downarrow$ fermions, are conserved separately. This is no longer true for $K \neq 0$ when coupling between states with the same parity of $N_\uparrow - N_\downarrow$ is present in the system. The value of $N_\uparrow - N_\downarrow$ depends on $N = N_\uparrow + N_\downarrow$; we have $N_\uparrow - N_\downarrow$ even for $L = 6, 8$ and odd for $L = 7$. The conservation of the total number of particles implies lack of coupling between the

Hilbert space spanned by vectors corresponding to $N_\uparrow - N_\downarrow$ being odd or even.

Additionally, the nonzero γ—responsible for the synthetic flux—breaks the TRI of the situation studied. Without the "symmetry-breaking" terms in the Hamiltonian, e.g., Eq. (2), this still results in the existence of the so-called generalized TRI [46] which we study below.

We use an exact diagonalization for different system sizes and flux quanta obtaining both spectral and time evolution properties of systems studied. While using more sophisticated techniques, one could extend the study to slightly larger systems (we estimate that the top shift-and-invert technique [47] could allow us to reach $L = 10$ with unit filling), we restrict ourselves in this exploratory work to small $L \leqslant 8$ systems amenable to an exact diagonalization. We estimate the influence of finite-size effects on our results by comparison with smaller system sizes. While the question of a possible instability of MBL phase in thermodynamic limit is debated [48–51], we believe that our results are robust on experimentally relevant timescales of several hundreds of tunneling times and for necessarily finite system sizes in cold atom implementations [52,53].

III. SPECTRAL STATISTICS

We consider first the statistical spectral properties of the model. A widely used signature of localization properties of a many-body system is the so-called gap ratio statistics [9]. From the eigenvalue spectrum of the many-body Hamiltonian, one computes the average gap ratio $\langle r \rangle$, where $r_n = \min(\delta E_n, \delta E_{n+1})/\max(\delta E_n, \delta E_{n+1})$ with E_n being the energy levels and $\delta E_n = E_{n+1} - E_n$ is the spacing between two consecutive eigenvalues. It turns out that the mean gap ratio may be correlated with the localization properties of eigenstates. For a localized system described by the Poisson-level statistics, the mean gap ratio is $\langle r_{\rm Poisson} \rangle = 2\ln 2 - 1 \approx 0.3863$; whereas the ergodic system is described by $\langle r \rangle$, corresponding to GOE $\langle r_{\rm GOE} \rangle = 0.5306$ for the real Hamiltonian matrix and GUE $\langle r_{\rm GUE} \rangle = 0.5996$ in the absence of (the generalized) time-reversal symmetry [54]. The mean gap ratio may depend on energy (e.g., for systems with the mobility edge) [10,55–57], thus it should be determined in the interval of energies where one expects the dynamics to be similar. Thus, from now on, we average r_n over the states lying in the center of the spectrum for which $\epsilon_n \equiv (E_n - E_{\rm min})/(E_{\rm max} - E_{\rm min}) \approx 0.5$, where $E_{\rm min}$ and $E_{\rm max}$ are the smallest and largest eigenvalues for a given disorder realization. For $L = 6, 7, 8$, we take 100,350,500 eigenvalues for each disorder realization, respectively. Finally, we average the obtained r_n over disorder realizations – we use over 5000, 2000, 500 realizations of disorder for $L = 6, 7, 8$, respectively.

Such a mean gap ratio as a function of disorder strength for Hamiltonian Eq. (1) is shown in Fig. 2. The on-site interaction is fixed at $U = 1$. Consider first the $\gamma = 0$ case—then the TRI in Hamiltonian Eq. (1) is preserved. Without the symmetry-breaking term, Hamiltonian Eq. (2), the individual spectra from diagonalizations consist of independent subsets of eigenvalues due to conserved quantities. Hence, the value of the average gap ratio $\langle r \rangle$ is close to the Poisson value

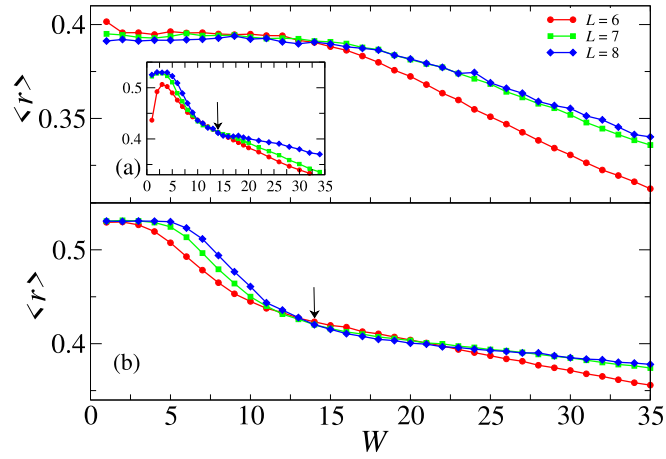

FIG. 2. Mean gap ratio $\langle r \rangle$ around the center of the spectra $\epsilon \approx 0.5$ as a function of disorder strength W for TRI case of $K = 1$, $\gamma = 0$ of Hamiltonian Eq. (1) in the absence (a) or in the presence (b) of the symmetry-breaking local term Eq. (2) for $h_b = 0.5$. The overlapping distinct spectra in case (a) lead to almost Poissonian-level statistics for any W (main figure). The inset in (a) shows that diagonalization of a single symmetry block of the Hamiltonian allows us to observe the crossover between GOE-like behavior at low W to Poisson statistics for larger W. The crossing of curves for $L = 7$ and $L = 8$ (indicated by an arrow) suggests a crossover transition value $W_c \approx 14$.

for arbitrary disorder strength W vis. [Fig. 2(a)]. To observe the transition between ergodic and MBL phases, we use the explicit forms of generators of SU(2) symmetry:

$$S^z = \frac{1}{2}\sum_j (\hat{n}_{j,\uparrow} - \hat{n}_{j,\downarrow}), \quad S^+ = (S^-)^\dagger = \sum_j \hat{c}^\dagger_{j,\uparrow}\hat{c}_{j,\downarrow}, \quad (3)$$

$$S^2 = \frac{1}{2}(S^+S^- + S^-S^+) + (S^z)^2. \quad (4)$$

For $K = 1$, the total number of up/down fermions, $N_\uparrow/N_\downarrow$ is not conserved and $[\hat{H}_0, S^z] \neq 0$. However, the Hamiltonian still commutes with $S^x = (S^+ + S^-)/2$ and S^2 operators, as can be checked by a direct calculation. Finding the Hamiltonian matrix in a basis composed of eigenstates of S^2 and S^x and performing exact diagonalization within a single block of the matrix, we explicitly observe the crossover between ergodic and MBL regimes as demonstrated in the inset of Fig. 2(a).

Alternatively, the crossover can be observed by applying the symmetry-breaking local Hamiltonian Eq. (2) [25]; indeed, as Fig. 2(b) demonstrates at weak W, $\langle r \rangle$ reaches the value $\langle r_{\rm GOE} \rangle$, while at strong disorder it approaches $\langle r_{\rm Poisson} \rangle$. This indicates the existence of two phases at $\gamma = 0$.

It would be tempting to extract the critical disorder strength W_c using finite-size scaling approach. We refrain from doing this for a few reasons. First, system sizes considered are quite small, so extrapolation to infinite system size must be doubtful. Even more importantly, the finite-size scaling analysis of MBL transition in spin chains (see, e.g., Ref. [10]) leads typically to critical exponent ν which breaks the Harris bound, which is 2 for one-dimensional systems [58]. The possible explanations may be related to the character of the transition resembling a Kosterlitz-Thouless transition [59]

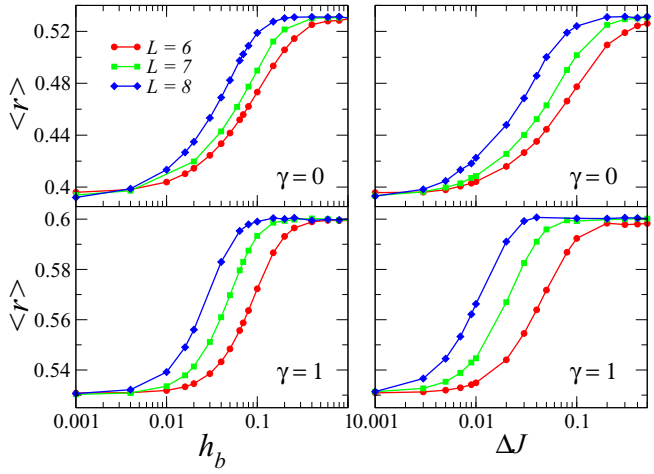

FIG. 3. Mean gap ratio for different system sizes in the delocalized regime ($W = 3$) as a function of the strength of the symmetry-breaking local magnetic field (left) or the difference between tunneling rates for spin-up and -down fermions (right), which also breaks the symmetry. The top row represents TRI case, $\gamma = 0$, where presence of symmetries results in a superposition of independent spectra yielding Poisson-like statistics. For complex fluxes, the residual reflection symmetry between spin-up and -down fermions (for unit filling) combined with TRI leads to generalized time-reversal symmetry (see discussion in the text), leading to an apparent GOE-like behavior. Only breaking this symmetry by a local field or difference in tunneling rates, the GUE-like statistics corresponding to broken TRI is observed.

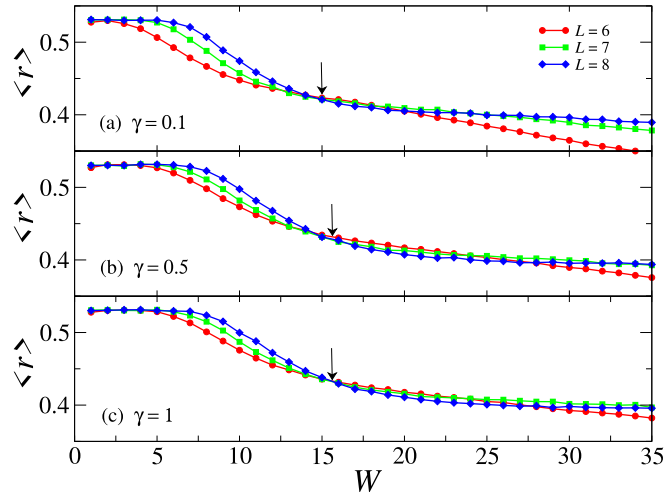

FIG. 4. Transition from GOE-like to Poissonian behavior, i.e., from delocalized to localized regime for Hamiltonian Eq. (1) possessing, for $\gamma > 0$, a generalized time-reversal symmetry for different values of γ as indicated in the figure. Observe that the crossover point between phases does not depend on γ.

with important logarithmic corrections. It has been suggested recently that, most likely, an asymmetric scaling governs the transition, which may carry over to all observables [60], see also Ref. [61].

In view of these problems, we tentatively identify the disorder strength W_c, beyond which the system becomes localized by the crossing of $\langle r \rangle$ curves for the largest available system sizes. That leads to $W_c \approx 14$ for $K = 1$ $\gamma = 0$, i.e., a TRI situation.

The remaining symmetries of Hamiltonian Eq. (1) for the TRI case ($\gamma = 0$) may be alternatively removed by making the tunneling J spin dependent, i.e., $J_\uparrow = J_\downarrow + \Delta J$. Both cases are visualized in Fig. 3, top row. At $W = 3$, the system is characterized by an almost Poissonian mean gap ratio in the presence of symmetries. The finite value of h_b couples different symmetry classes and reveals the true extended character of the system with $\langle r \rangle$ corresponding to GOE (top left panel). A very similar behavior is observed when spin-dependent tunneling is present (top right panel). In both cases, the larger the system, the smaller the value of the symmetry-breaking parameter required to fully break symmetry constrains.

Let us now consider the case of nonvanishing phase γ in tunnelings—compare Hamiltonian Eq. (1). Nonzero γ breaks a standard TRI—one might naively expect in that case the GUE-like behavior in the delocalized regime. Yet, as shown in the bottom row in Fig. 3, without h_b (or spin-dependent tunneling) the mean gap ratio $\langle r \rangle \approx 0.53$ points toward GOE statistics. This is explained by the fact that while standard TRI is broken, there exists a generalized TRI in our system Eq. (1), namely, TRI combined with reflection in $x - y$ plane (i.e., change of the spin direction). That generalized TRI leads to GOE statistics (for an excellent discussion of symmetries in different universality classes see Ref. [46]).

With the introduction of h_b or spin-dependent tunneling, this generalized TRI symmetry is broken and, once the symmetry is fully broken, the GUE statistics is fully recovered in the delocalized regime as shown in the bottom row of Fig. 3.

Consider now the crossover from the delocalized to localized regime for nonzero γ, i.e., in the presence of a synthetic field. Let us discuss first the case with $h_b = 0$ and a generalized TRI—compare Fig. 4. Please note that the observed GOE–Poisson transition in mean gap ratio values seems not to depend on γ (once it is sufficiently big to mix different symmetry sectors) as we observe examining the crossing points of curves in Fig. 4 for system sizes $L = 7, 8$.

On the contrary, in the presence of the additional local field [i.e., adding the term Eq. (2) to the Hamiltonian Eq. (1)], the transition between GUE and Poisson-like behavior becomes dependent on γ as apparent from data presented in Fig. 5. One might think that this shift of the transition is related to the way in which the symmetry is broken, namely, by a local magnetic field. Such a local perturbation might differently affect the transition to the localized phase for different value of γ. However, we have checked, by adding random fields on all of the lattice sites, that this is not the case.

A possible explanation is the following. Consider first the transition between GOE and Poisson-level statistics in the absence of the symmetry-breaking field as in Fig. 4. The Hamiltonian of the system Eq. (1) for $\gamma > 0$ is a complex matrix in the basis of Fock states $|FS_j\rangle$. Constructing a unitary matrix U_P such that

$$U_P|FS_j\rangle = \frac{e^{i\phi_j}}{\sqrt{2}}(|FS_j\rangle + i\mathcal{P}|FS_j\rangle),$$
$$U_P(\mathcal{P}|FS_j\rangle) = \frac{e^{i\phi_j}}{\sqrt{2}}(i|FS_j\rangle + \mathcal{P}|FS_j\rangle), \quad (5)$$

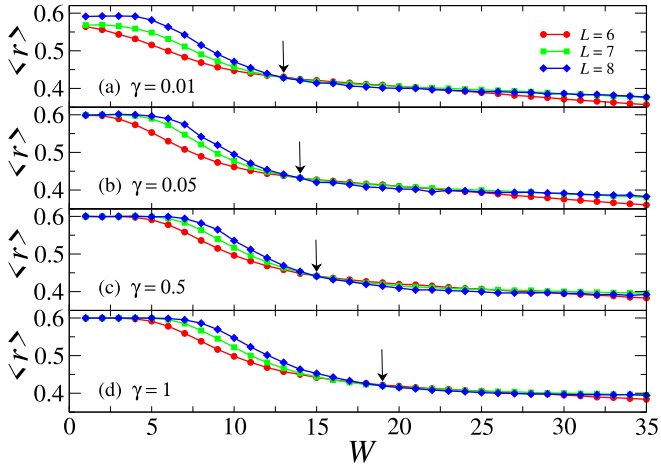

FIG. 5. Transition from GUE-like to Poissonian behavior, i.e., from delocalized to localized regime for Hamiltonian Eq. (1) with additional symmetry breaking term Eq. (2) with $h_b = 0.5$. Contrary to $h_b = 0$ case presented in Fig. 4, now the crossover point between phases significantly depends on γ.

where $\mathcal{P}$ is the parity operator (changing up to down spins and vice versa), we verify numerically that an appropriate choice of phases ϕ_j leads to a purely real matrix $H' = U_P^\dagger H_0 U_P$. The transformed Hamiltonian matrix H' has the following properties:

(i) Diagonal entries of matrix H_0 are equal to corresponding diagonal matrix elements of H'.

(ii) Off-diagonal entries of H_0 due to hopping along the leg of the ladder correspond to off-diagonal entries of H' of the same number and magnitude

(iii) Off-diagonal entries $e^{i\gamma j}$ of H_0 due to hopping in the synthetic dimension become off-diagonal real entries $K[\pm\cos(\alpha\gamma) + \sin(\beta\gamma)]$ of H', where α, β are integer numbers lying in the interval $(-L, L)$.

Figure 6 shows distributions $P(m)$ of off-diagonal entries m of the Hamiltonian matrix H'. For $1 \ll \gamma > 0$, the distribution

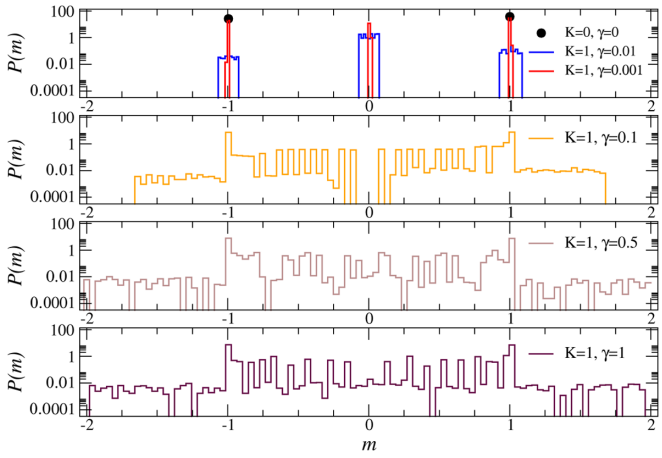

FIG. 6. The distribution of off-diagonal entries of matrix H' for various values of parameters K and γ for the system size $L = 8$. Once γ is larger than $\approx$0.1, the distribution is only weakly dependent on the value of γ.

has peaks concentrated at $m = \pm 1, 0$. As the value of γ increases the distribution, $P(m)$ broadens due to the off-diagonal matrix elements associated with tunneling in the synthetic dimension (iii). For values of γ larger than the certain system-size-dependent γ_0, the distribution $P(m)$ changes only mildly with γ. Since the diagonal entries of the matrix remain intact, it seems plausible that the independence of the crossover point of the value of γ observed in Fig. 4 is caused by the fact that the distribution of off-diagonal entries does not change significantly once $\gamma \gtrsim 0.1$ for system size $L = 8$.

The properties of the crossover in the presence of the additional symmetry-breaking field, e.g., $h_b = 0.5$ as in Fig. 5, are starkly different—the position of crossover shifts with γ, especially for $\gamma > \gamma_0$. Viewing $H_{\rm sb}$ Eq. (2) as a perturbation to eigenstates of H_0, we see that even though the overall properties of the unperturbed system change with disorder strength W independently of γ (provided that $\gamma > \gamma_0$), the eigenstates depend on the value of γ. This conclusion is further corroborated in the study of eigenstate properties in Sec. VII.

IV. DYNAMICS AND DENSITY CORRELATIONS

To study the dynamical properties, we choose random Fock state $|\psi(0)\rangle$ as an initial state for the temporal evolution and examine the dynamics of the local correlations and the entanglement entropy for $L = 8$. The local charge and spin correlations are $C(t) = A\sum_j \langle \rho_j(t)\rho_j(0)\rangle$ and $S(t) = B\sum_j \langle m_j(t)m_j(0)\rangle$, where $\rho_j = n_j - \bar{n}$ with the average density $\bar{n} = \sum_j n_j/L$, and A and B are normalization constants such that $C(0) = S(0) = 1$. Recall that n_j (m_j) are the sum (difference) of the site occupations of up- and down-polarized fermions, respectively. We assume a unit filling, $\bar{n} = 1$.

Let us recall what is known about the disordered Hubbard case, $K = 0$. The memory of the initial state is lost for sufficiently small disorder. The system is delocalized and this leads to the decay of charge and spin correlations. An interesting situation occurs for stronger disorder where (in the absence of symmetry breaking local magnetic field or other effects destroying the system symmetries) the charge sector appears localized but spin sector does not show localization [29,32]. The absence of a fully localized phase is due to the SU(2) symmetry of the model. The choice of a different random potential for up- and down-polarized fermions, a random magnetic field or a weak spin asymmetry which breaks the SU(2) spin symmetry recovers the full MBL phase [31,34,35]. For the Hubbard model, the subdiffusive transport of spins can be traced back to a singular random distribution of effective spin exchange interactions [30] and at long times the transport is strongly suppressed [32]. The particle transport rate is exponentially small in J/W, and the rate depends strongly on the initial state of the system. The states occupied with only doublons or holons exhibit full MBL phases as for such states where the delocalization rate is zero [33]. This is the current understanding of dynamical properties of disordered Hubbard model.

Considering the coupling of spin-up and -down particles allows for further studies of ergodicity breaking in the model. We concentrate mostly on the strongly disordered regime where either charge or spin correlations decay very slowly on

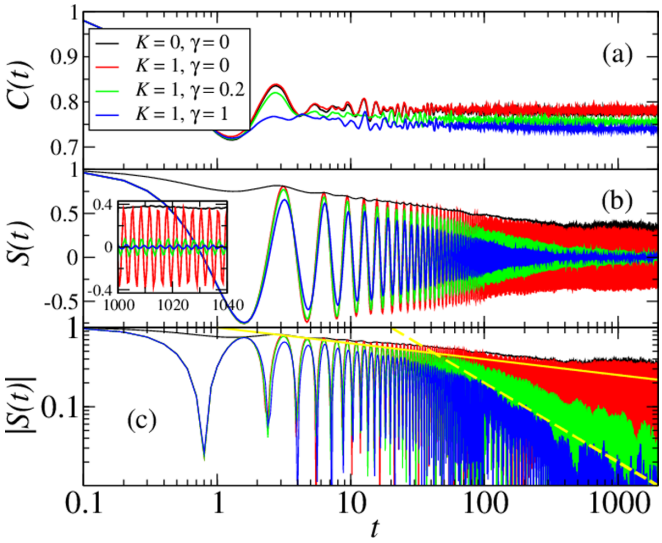

FIG. 7. Time evolution of the local charge and spin correlations of random Fock states for $U = 1$, $W = 32$, and $h_b = 0$. (a) The charge remains localized in the presence of the synthetic flux. (b) In the absence of the flux, when $K = 0$, the spin delocalizes with subdiffusive decay of correlations (see text for discussion). Once K is finite, the spins oscillate (red curve) and the $S(t)$ of $K = 0$ (black curve) provides an envelope to these oscillations. This is apparent from the inset plot where the oscillations in the evolution at large times are shown. At $\gamma > 0$, the oscillations are damped and $S(t)$ decays to zero. The gauge field delocalizes the spins. (c) The modulus of $S(t)$ in the log-log scale. Yellow line proportional to $1/t^{0.2}$ shows the subdiffusive character of decay for $K = 0$. The decay becomes faster and for $K = \gamma = 1$ becomes ballisticlike with $1/t$ behavior as exemplified by a dashed yellow line. The average is performed for 300 disorder realizations.

the timescale considered—we study the dynamics up to $t = 2000/J$, which seems to be at the edge of current experimental possibilities with cold atomic setups. The time evolution of density and spin correlations are shown in Fig. 7. We examine the behavior of correlations at several values of the synthetic flux to observe its influence on the dynamics. For $\gamma = 0$, $K = 0$ (i.e., no coupling between the up- and down-polarized fermions), the charge correlation $C(t)$ saturates at a finite value for an exemplary $W = 32$ value. The spin correlation $S(t)$ shows a slow decay claimed in earlier works to be due to subdiffusive spin transport [29–32]. Figure 7(c) shows the decay of spin correlations in the log scale; observe that the decay up to time $t \approx 300$ follows a power law, $|S(t)| \propto 1/t^{0.2}$, then the slope of the curve diminishes. It is worth noting that a similar behavior was observed for a much larger system in Ref. [32].

Also at zero flux ($\gamma = 0$), the coupling of spin degrees of freedom through finite hopping along the synthetic dimension ($K = 1$) does not alter the behavior of $C(t)$ and the charge remains localized on the timescale considered. In the presence of a finite synthetic flux $\gamma = 0.2$ and 1, after a transient time of the order of $1/J$, the charge again seems to saturate. Yet a careful analysis of $C(t)$ reveals a residual very slow algebraic decay, $C(t) \propto t^{-\alpha}$ with $\alpha = 0.004(2)$ for $K = \gamma = 1$ as compared to an order of magnitude less α for $\gamma = 0$. Since this power is quite small, we have performed detailed tests using the bootstrap technique to analyze the error (1150 disorder realizations are used). $\alpha = 0.004(2)$ is obtained when fitting the decay over $t \in [100, 200]$. Fitting the slope, we observe that α decreases with time, e.g., $\alpha = 0.0021(3)$ in the interval $t \in [200, 1000]$, suggesting that the decay is slower than the power law. Also, $\alpha = 0.004$ is significantly smaller than the exponent governing residual decay of imbalance at MBL transition in large systems of spinless fermions [62,63]; thus, we believe that a small value of α indicates that the charge sector of spinful fermions remains localized in the presence of the synthetic gauge field for a sufficiently strong disorder. Let us also note that the power of the small residual decay is also dependent on the system size increasing with it, e.g., we get $\alpha = 0.0032(7)$ for $t \in [100, 200]$ for $L = 7$.

Consider now the evolution of the spin correlation $S(t)$, which is shown in Fig. 7(b). In the absence of the flux, $S(t)$ decays slowly in agreement with the subdiffusive manner suggested in such a case [30–32]. As in the study of much larger system sizes [32] for times up to around $t = 300 - 350$, the decay is faster with a power law character $t^{-0.175(1)}$ slowing down at large times to $t^{-0.037(2)}$. As discussed in Ref. [32], the functional dependence of the decay in the $t \in (300, 2000)$ interval is hard to determine numerically (equally well, one might assume a logarithmic dependence). Powers of decay slower than $1/2$ suggest a subdiffusive behavior [64] as proposed [30,31].

The presence of coupling between the legs of the ladder $K > 0$ strongly affects the spin dynamics—$S(t)$ becomes oscillating. The frequency of oscillations is simply $K/2$ as may be verified inspecting the inset of Fig. 7(b). Interestingly, the oscillations have the envelope given by the $S(t)$ curve for $K = 0$. This quite surprising observation may be easily explained. Denote by H_K the term of H_0 proportional to K and by $H_H = H_0 - H_K$. We verify that $[H_H, H_K] = 0$ as long as $\gamma = 0$. Thus, the evolution operator factorizes: $\exp(-iH_0 t) = \exp(-iH_H t)\exp(-iH_K t)$ and the average number of fermions with spin σ at site j is given by

$$n_{j\sigma}(t) = \langle\psi(0)|e^{iH_H t}e^{iH_K t}\hat{n}_{j\sigma}e^{-iH_K t}e^{-iH_H t}|\psi(0)\rangle, \quad (6)$$

so the time evolution of spin-correlation function is a superposition of dynamics determined by the H_H Hamiltonian and oscillations driven by the H_K term. The long-time average of the oscillations is zero, which is in agreement with a previous study on the localization of coupled chains with correlated disorder [65].

In the presence of a finite flux, $[H_K, H_H] \neq 0$, the oscillations are damped and the damping rate grows with γ. Thus, the spin sector of the system gets delocalized by the introduction of gauge field. The decay of spin-correlation function changes from the subdiffusive at $\gamma = 0$, continuously reaching $1/t$ behavior at $\gamma = 1$ characteristic for a ballisticlike motion [64]—compare Fig. 7(c).

To examine the effect of quantum statistics, we further analyze the time dependence of local correlations when instead of fermions we consider hard-core bosons in the Hamiltonian Eq. (1). A cold atom implementation might use ^{39}K instead of ^{40}K, also with Zeeman sublevels. Using well-controlled Feshbach resonances [66], one may increase interactions between bosons to a degree when double occupations in the

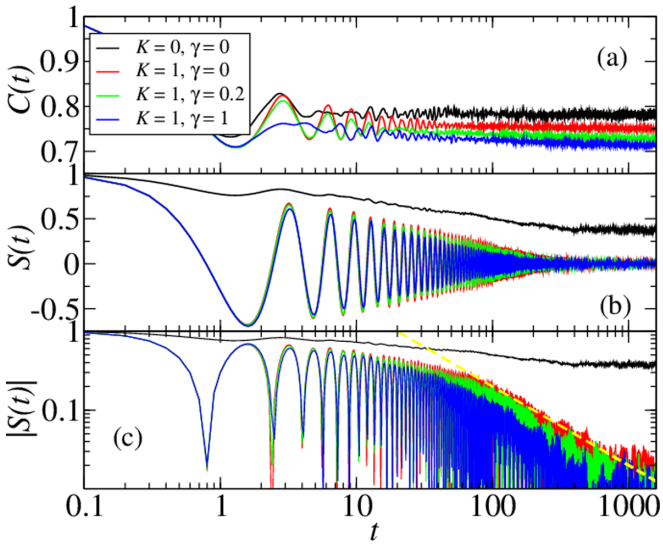

FIG. 8. The local correlations of the hard-core bosons in the localized regime $W = 32$. The initial states are the random Fock states and $U = 1$. (a) The charge remains localized in the presence of gauge field. (b) Once the tunneling coupling K between up and down spins is turned on, the spin correlations decay to zero, showing transient oscillations with $K/2$ frequency. The decay of the envelope seems to be ballisticlike at longer times—a dashed bright (yellow online) line in panel (c) indicates $1/t$ decay.

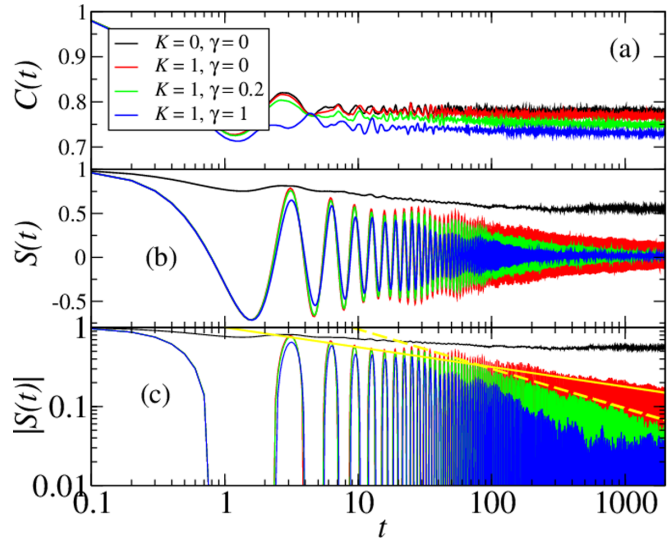

FIG. 9. Same as Fig. 7 but in the additional presence of the local magnetic field term [Eq. (2)] breaking the generalized TRI symmetry. The strength of local field $h_b = 0.5$. The presence of coupling K induces faster decay of $S(t)$ as compared to the case without symmetry breaking local field [Fig. 7—still the decay is subdiffusive as indicated by a solid bright (yellow) line with slope $1/t^{0.25}$]. In the presence of the flux, the decay is faster, approximately diffusive for $\gamma = 0.2$—see the yellow dashed line proportional to $1/\sqrt{(t)}$, for larger γ becoming even faster.

lattice become energetically prohibited, realizing hard-core boson limit. The correlations of hard-core bosons for different values of K and γ are shown in Fig. 8. For $K = 0$, i.e., no phase-sensitive coupling between the legs of the ladder, both charge and spin correlations behave similar to the fermionic case. The situation changes for $K > 0$. The behavior of charge correlation, $C(t)$, is similar to the fermionic case and its finite saturation value indicates the localization of the charge sector in the presence of the synthetic flux. The saturation value of $C(t)$ decreases with $0 \leqslant \gamma \leqslant 1$ at $K = 1$. The spin sector behaves differently. The coupling of two hyperfine states (along the rungs of the ladder), even for $\gamma = 0$, leads to oscillations of spin correlations, which in contrast to fermionic $S(t)$, are damped to zero. This is due to the fact that the commutator $[H_K, H_H] \neq 0$ for hard-core bosons, leading to the damping of $S(t)$. A finite flux γ only weakly affects the damping, and the spin sector becomes fully delocalized. The decay of spin correlations seems almost exponential at first. Then, at later times, as indicated by the yellow dashed line in Fig. 8(c), the decay of spin correlations is ballisticlike, i.e., governed by $1/t$ behavior independently of the flux γ. The stark contrast of $S(t)$ between hard-core bosons and fermions for $K = 1$ and $\gamma = 0$ is a very nice demonstration of effects induced by quantum statistics and different commutation properties of fermions and hard-core bosons (for ground-state properties, this observation goes back to Ref. [67]).

Finally, we return to the fermionic system and calculate time evolution of charge- and spin-correlation functions as shown in Fig. 9 for nonzero value of symmetry-breaking field h_b. In this case, even at $\gamma = 0$, the commutator $[H_H + H_{\rm sb}, H_K] \neq 0$ and the oscillations of $S(t)$ are damped. The effects of broken generalized TRI symmetry, while altering significantly spectral properties of the system, have a relatively small effect on time dynamics of the charge correlation function $C(t)$ for $\gamma > 0$. On the other hand, for spin-correlation function $S(t)$, we again observe a transition from a subdiffusive (at nonzero K and zero flux) to superdiffusive (for sufficiently large flux γ) decay of the spin-correlation function.

V. ENTANGLEMENT ENTROPY GROWTH

To corroborate our study of spin delocalization in the presence of the synthetic gauge field, we investigate the entanglement entropy growth in the system. The two-leg ladder system can be partitioned in several ways with two prime options: The first one is to cut the ladder perpendicular to the direction of the spatial dimension in two equal (left-right) parts and the second one is to cut the ladder perpendicular to the direction of synthetic dimension decoupling the hyperfine states. This allows us to study both the entanglement between two left and right ladder subsystems but also between an ensemble of up- and down-polarized fermions.

Regardless of the splitting, the von Neumann entanglement entropy is defined in a standard way as

$$S_E(t) = -\mathrm{Tr}\rho_A(t)\ln\rho_A(t), \tag{7}$$

where the two subsystems are denoted as A and B with $\rho_A(t) = \mathrm{Tr}_B|\psi(t)\rangle\langle\psi(t)|$ being the reduced density matrix of subsystem A. Here Tr_B is the trace over degrees of freedom of subsystem B.

In the MBL regime, the entropy of entanglement of initially separable states should grow logarithmically in time [23,24]

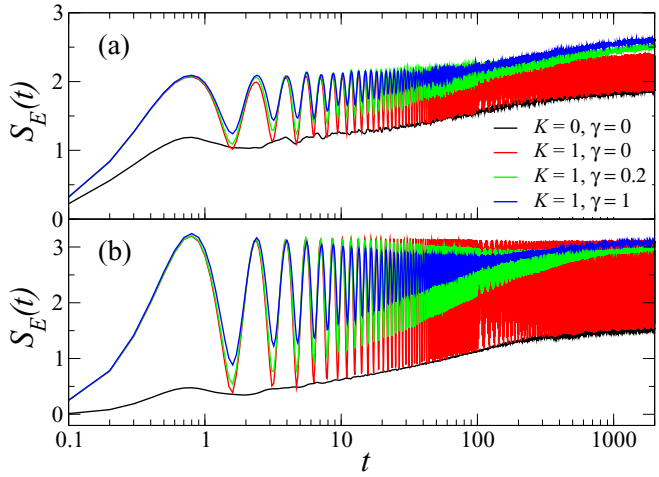

FIG. 10. (a) Left-right bipartite entanglement entropy in the localized regime. With no coupling of spin-up and spin-down polarized fermions, a typical logarithmic growth of S_E is observed after initial transients. Coupling K induces oscillations of the entanglement entropy. Complex flux γ leads to damping of these oscillations with also faster entropy growth. (b) Bipartite entanglement entropy dynamics when rungs of the ladder are cut, i.e., a partition divided up- and down-polarized fermions.

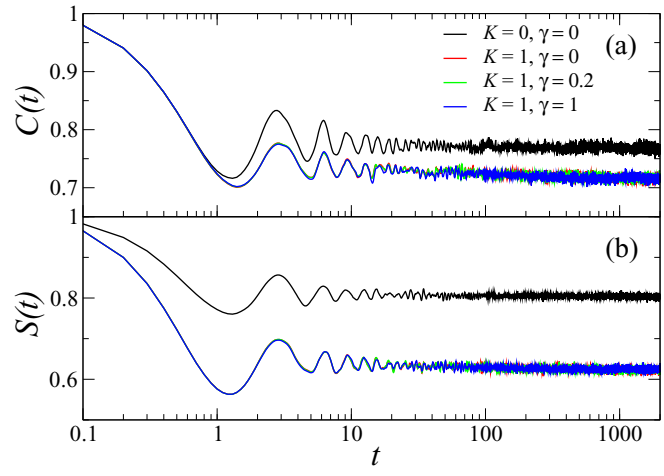

FIG. 11. (a) Charge $C(t)$ and (b) spin $S(t)$ correlation functions for uncorrelated disorder $\epsilon_{j\sigma} \in [-W/2, W/2]$, the chemical potential is site and spin dependent. The system size is $L = 8$, disorder strength $W = 32$, various values of coupling K and flux γ are considered. Both $C(t)$ and $S(t)$ saturate signaling localization of both charge and spin sectors.

after an initial transient eventually saturating for a finite system size [24]. Such a behavior is indeed observed in our model for decoupled spin chains ($K = \gamma = 0$) both for the standard left-right splitting [Fig. 10(a)] and for the up-down splitting [Fig. 10(b)].

The coupling between up- and down-polarized fermions introduces strong oscillations in the entanglement entropy, with the same period as revealed by the spin-correlation function—compare Fig. 10(a). Similarly, the entropy curve for $K = 0$ forms an envelope (here low-lying envelope) to the oscillations. Again, this fact is related to vanishing commutators between different kinetic energy terms in the Hamiltonian Eq. (1), as described in the previous section. The presence of complex flux makes these commutators nonzero and introduces the damping of the oscillations. The resulting entropy growth is significantly faster than in the $K = \gamma = 0$ case, reflecting the delocalization of spin sector.

Similarly, even more spectacular oscillations of the entanglement entropy are observed when the partition divides up- and down-polarized fermions (i.e., the rungs in the ladder are cut). The coupling between up and down fermions ($K = 1$) makes the entropy oscillate maximally, with the lower envelope given by the $K = 0$ curve as before, while the upper envelope is system-size and disorder-strength dependent. Again, the nonzero flux introduces damping of these oscillations—on the timescale discussed, the entropy growth practically saturates at the upper allowed value [Fig. 10(b)].

VI. SPIN-DEPENDENT DISORDER

Up till now, we have considered the disorder identical for both spin components. Such a situation (albeit for quasiperiodic disorder) is realized in experiments [5]. However, it is possible (and feasible) experimentally to consider a situation when disorder is different (and uncorrelated) for both spin components with the last term in $\hat{H}_H$ of Hamiltonian Eq. (1) being changed to $\sum_{j,\sigma} \epsilon_{j,\sigma} \hat{n}_{j,\sigma}$, where now $\epsilon_{j,\sigma}$ are independent random variables drawn from uniform distribution in the interval $[-W/2, W/2]$. The resulting charge- and spin-correlation functions are shown in Fig. 11. We observe a clear localization of both charge and spin sectors as $C(t)$ and $S(t)$ saturate to constant values after initial oscillations. The fact that the addition of a (small amount of) disorder in spin sector, in the presence of strong charge disorder, is sufficient to fully localize the system was also observed in Ref. [35]. The saturation values are lower for $K = 1$ than for $K = 0$ and, interestingly, are independent of the flux γ.

To complete the picture, we consider the case of spin disorder, namely, we replace the last term in $\hat{H}_H$ of Hamiltonian Eq. (1) by $\sum_j \epsilon_j (\hat{n}_{j,\uparrow} - \hat{n}_{j,\downarrow})$ so the disorder affects the spin degree of freedom. In this case, for $K = 0$, the system possesses pseudospin SU(2) symmetry that can be utilized in studies of its localization properties [68]. Charge- and spin-correlation functions for various values of K and γ are shown in Fig. 12. We observe that the spin sector is localized as $S(t)$ quickly saturate whereas the charge correlations decay, suggesting delocalization of charge degrees of freedom.

Note that when disorder becomes spin dependent, the time evolution of both charge- and spin-correlation functions is no longer dependent on the phase of the coupling γ between spin components. While, for individual realizations of disorder, the evolution may differ substantially, the differences average out when taking the disorder average. Once the spin degree of freedom becomes localized, the information transfer between the legs of the ladder stops regardless of γ value. It is worth mentioning that similar independence of the flux is also observed in the entanglement entropy for uncorrelated and spin disorder.

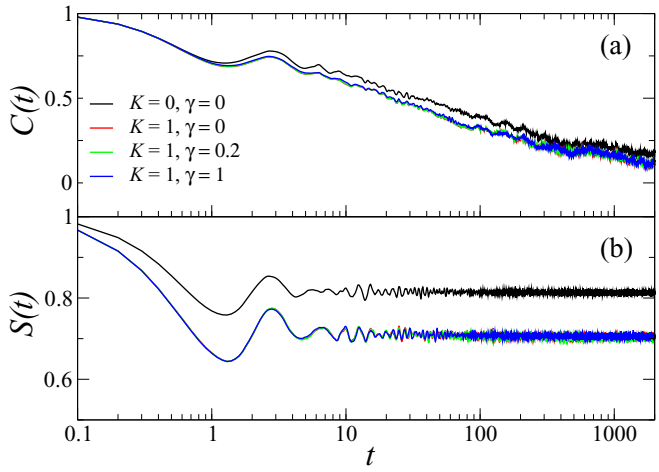

FIG. 12. (a) Charge $C(t)$ and (b) spin $S(t)$ correlation functions for spin disorder $\epsilon_{j\sigma} = -\epsilon_{j\bar{\sigma}}$ (where $\bar{\sigma}$ denotes spin opposite to σ). The system size is $L = 8$, disorder strength $W = 32$, various values of coupling K, and flux γ are considered. The saturation of $S(t)$ signals localization of the spin sector whereas the charge sector remains delocalized.

VII. PARTICIPATION RATIO

One may make the observation that the disorder-averaged quantities do not depend on the synthetic flux even stronger. Consider the participation ratio of nth eigenstate $|n\rangle$,

$$\mathcal{P}R_n = 1/\sum_i |\langle n|b_i\rangle|^4, \tag{8}$$

where $|b_i\rangle$ are basis functions (we chose a natural basis of Fock states on lattice sites). We denote as PR_n the participation ratio of level n averaged over disorder realizations. For identical random disorder for both spin components [Hamiltonian Eq. (1)], PR defined in this way depends on K and γ—compare Fig. 13(a). Significant values of PR suggest that localization is not complete. For the disorder uncorrelated between spin components with the same amplitude W, we observe significantly smaller PR (pointing toward stronger localization), moreover, PR becomes independent of γ (recall that PR_n are obtained after disorder averaging). Thus, not only $C(t)$ or $S(t)$ but also other observables may be expected to be γ independent once the spin component is localized.

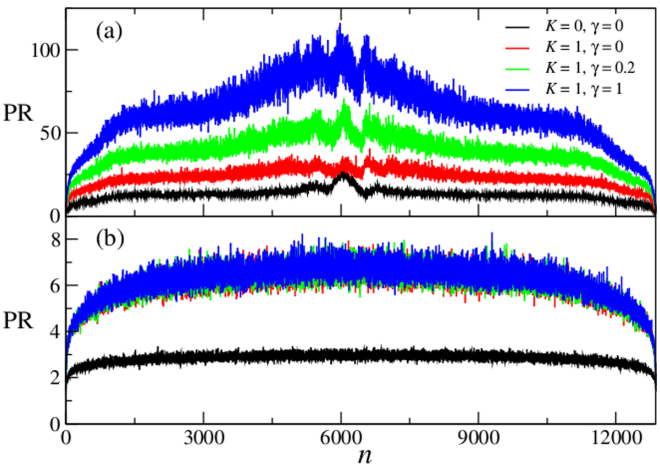

FIG. 13. Averaged-over-disorder realization participation ratio (a) for Hamiltonian Eq. (1) and (b) for disorder uncorrelated between spin components, leading to full MBL of both charge and spin.

In this respect, we observe a clear asymmetry between a real dimension (along the chain) and the synthetic dimension (represented by spin components). The localization of the latter is essential for γ independence of disorder-averaged observables while the charge localization plays little role. Observe that for pure spin disorder, as shown in Fig. 12, the correlations for $K = 1$ are flux independent while charge degrees of freedom are delocalized.

The conclusions drawn from participation ratios at a given system size may be qualitative only; it is important to study their behavior as a function of the system size as described, e.g., in Ref. [60]. Following the prescription of Ref. [60], we define the participation entropy $S_2(n) = \ln \mathcal{P}R_n = -\ln \sum_i |\langle n|b_i\rangle|^4$, where the latter equality gives a relation of S_2 with the inverse of the participation ratio Eq. (8), commonly known as the inverse participation ratio. For states in the middle of the spectrum, we define $\overline{S_2}$ as an average over both the different levels and the disorder realizations and refer to it as a participation entropy. As shown in Ref. [60], one should consider how $\overline{S_2}$ behaves with the system size. In particular, for perfectly delocalized state $\overline{S_2} = \ln N$, where N is the Hilbert space dimension, while perfectly localized state $\overline{S_2}$ should be a constant independent of N. For spinless fermions, in the paradigmatic MBL system it was found [60] that $\overline{S_2}$ is well fitted by $\overline{S_2} = D \ln N + a$, finding in particular that, on the localized side $D \approx 0.088$ and $a > 0$ in the Fock basis we consider (the obvious drawback of the participation entropy is that it depends on the choice of basis). Together with other measures and considering much larger system sizes led the authors to conclude that eigenstates on the MBL side are not fully localized and reveal multifractal character.

Following this example, we looked at the scaling of $\overline{S_2}$ for different combinations of K and γ parameters as well as different disorder cases. Again we chose $W = 32$ and system sizes up to $L = 8$. The results are collected in Fig. 14. As for spinless fermions, the obtained participation entropy values increase linearly with $\ln N$. For full MBL, i.e., for independent disorder for up and down fermions, the slope of the lines is smallest with $D = 0.108(5)$ for a standard Hubbard case, i.e., for $K = \gamma = 0$. The presence of a gauge field $K = \gamma = 1$ increases D twice but the general trend remains the same. For the same disorder for up and down fermions (correlated disorder), the increase of $\overline{S_2}$ with $\ln N$ is faster but follows the same trend with $0 < D < 0.5$, which suggests the multifractal character of eigenvectors. We shall also note that the subleading free term a in all cases studied is positive as observed for a localized side of the transition [60].

The limited system sizes considered by us do not allow us to proceed further with a full finite-size scaling analysis. However, the data presented in Fig. 14 strongly suggest that the multifractal character of wave functions in spinless fermionic systems postulated by Ref. [60] similarly appears for spinfull fermions studied.

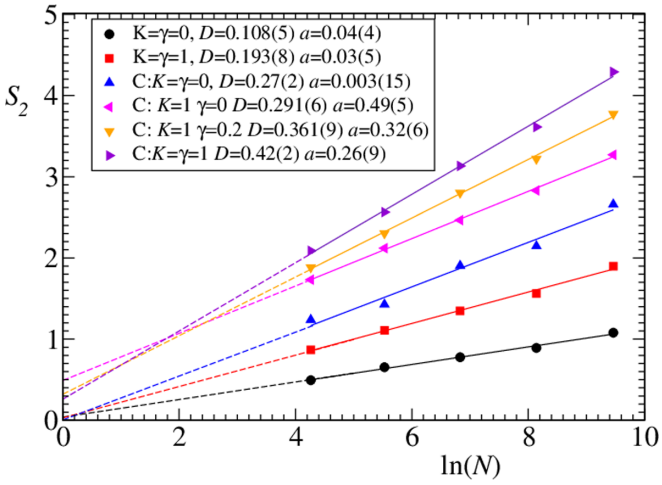

FIG. 14. Participation entropy, $\overline{S_2}$, as a function of the logarithm of Hilbert space dimension for different cases considered. Two low-lying lines show the linear dependence of $\overline{S_2}$ on $\ln(N)$ for independent disorder for up and down fermions, with TRI symmetry broken case given by red squares. The other four cases correspond to identical disorder for both legs (correlated disorder denoted by C in the legend). The leading slope D in all cases is lower than 0.5, indicating multifractal character of eigenvectors resembling the finding of Ref. [60].

VIII. CONCLUSIONS

We have analyzed properties of the disordered chain of spin-1/2 fermions in the presence of the synthetic magnetic field. While the spectral properties such as the average gap ratio indicate the transition to many-body localized phase, the time dynamics suggest that MBL is realized in the charge (density) sector only. The presence of the synthetic magnetic field delocalizes the spin sector as revealed by the decay of spin time correlation function. Similarly, the entropy of entanglement in the system grows much faster in the presence of the magnetic field flux.

Interestingly, the spectral properties of the system strongly depend on the realized symmetries, providing a nice example of the effects due to a generalized TRI (i.e., a TRI combined with a discrete symmetry). In effect, despite the standard time reversal symmetry being broken, the spectral properties in the delocalized regime resemble that of GOE unless additional symmetry breaking terms are introduced into the model.

A comparison of the dynamics of correlation functions for fermions and hard-core bosons in the absence of the flux ($\gamma = 0$) but when the driving term K couples up- and down-polarized particles shows sensitivity of the observed phenomena to quantum statistics. For fermions, due to their commutation relations, a kinetic energy part corresponding to the transition between spin-up and -down fermions commutes with the rest of the Hamiltonian. In effect, the exact quantum dynamics is given by a rapidly oscillating solution whose one envelope is given by $K = 0$ (i.e., no Rabi coupling) solution. This behavior is absent for hard-core bosons.

Last but not least, we considered different types of random disorder, in particular spin-dependent disorder that leads to strong localization in the spin sector. In such a case, time-dependent observables become, after disorder average, independent of flux γ. Analysis of participation ratio suggests the multifractal character of eigenvectors in the strong disorder regime also in the presence of artificial flux. We believe that the system sizes examined in present work are sufficient to grasp robust features of considered systems on timescales relevant for experiments with ultracold atoms.

ACKNOWLEDGMENTS

Interesting discussions with T. Chanda, D. Delande, and K. Życzkowski on subjects related to this work are acknowledged. The support by PL-Grid Infrastructure was important for this work. This research has been supported by National Science Centre (Poland) under Projects No. 2015/19/B/ST2/01028 (P.S.), No. 2018/28/T/ST2/00401 (doctoral scholarship—P.S.), and No. 2016/21/B/ST2/01086 (K.S. and J.Z.).

[1] L. Fleishman and P. W. Anderson, Phys. Rev. B **21**, 2366 (1980).
[2] F. Alet and N. Laflorencie, C. R. Phys. **19**, 498 (2018).
[3] S. A. Parameswaran and R. Vasseur, Rep. Prog. Phys. **81**, 082501 (2018).
[4] D. A. Abanin, E. Altman, I. Bloch, and M. Serbyn, Rev. Mod. Phys. **91**, 021001 (2019).
[5] M. Schreiber, S. S. Hodgman, P. Bordia, H. P. Lüschen, M. H. Fischer, R. Vosk, E. Altman, U. Schneider, and I. Bloch, Science **349**, 842 (2015).
[6] P. Bordia, H. P. Lüschen, S. S. Hodgman, M. Schreiber, I. Bloch, and U. Schneider, Phys. Rev. Lett. **116**, 140401 (2016).
[7] J. Smith, A. Lee, P. Richerme, B. Neyenhuis, P. W. Hess, P. Hauke, M. Heyl, D. A. Huse, and C. Monroe, Nat. Phys. **12**, 907 (2016).
[8] K. Xu, J.-J. Chen, Y. Zeng, Y.-R. Zhang, C. Song, W. Liu, Q. Guo, P. Zhang, D. Xu, H. Deng, K. Huang, H. Wang, X. Zhu, D. Zheng, and H. Fan, Phys. Rev. Lett. **120**, 050507 (2018).
[9] V. Oganesyan and D. A. Huse, Phys. Rev. B **75**, 155111 (2007).
[10] D. J. Luitz, N. Laflorencie, and F. Alet, Phys. Rev. B **91**, 081103(R) (2015).
[11] M. Serbyn and J. E. Moore, Phys. Rev. B **93**, 041424(R) (2016).
[12] R. Vasseur, A. J. Friedman, S. A. Parameswaran, and A. C. Potter, Phys. Rev. B **93**, 134207 (2016).
[13] A. Maksymov, P. Sierant, and J. Zakrzewski, Phys. Rev. B **99**, 224202 (2019).
[14] P. Sierant and J. Zakrzewski, Phys. Rev. B **99**, 104205 (2019).
[15] P. Sierant and J. Zakrzewski, Phys. Rev. B **101**, 104201 (2020).
[16] A. Pal and D. A. Huse, Phys. Rev. B **82**, 174411 (2010).
[17] M. Serbyn, Z. Papić, and D. A. Abanin, Phys. Rev. Lett. **111**, 127201 (2013).
[18] D. J. Luitz, N. Laflorencie, and F. Alet, Phys. Rev. B **93**, 060201(R) (2016).

[19] P. Sierant, D. Delande, and J. Zakrzewski, Phys. Rev. A **95**, 021601(R) (2017).

[20] K. Agarwal, S. Gopalakrishnan, M. Knap, M. Müller, and E. Demler, Phys. Rev. Lett. **114**, 160401 (2015).

[21] Y. Bar Lev, G. Cohen, and D. R. Reichman, Phys. Rev. Lett. **114**, 100601 (2015).

[22] M. Kozarzewski, P. Prelovšek, and M. Mierzejewski, Phys. Rev. B **93**, 235151 (2016).

[23] J. H. Bardarson, F. Pollmann, and J. E. Moore, Phys. Rev. Lett. **109**, 017202 (2012).

[24] M. Serbyn, Z. Papić, and D. A. Abanin, Phys. Rev. Lett. **110**, 260601 (2013).

[25] R. Mondaini and M. Rigol, Phys. Rev. A **92**, 041601(R) (2015).

[26] J.-y. Choi, S. Hild, J. Zeiher, P. Schauß, A. Rubio-Abadal, T. Yefsah, V. Khemani, D. A. Huse, I. Bloch, and C. Gross, Science **352**, 1547 (2016).

[27] H. P. Lüschen, P. Bordia, S. Scherg, F. Alet, E. Altman, U. Schneider, and I. Bloch, Phys. Rev. Lett. **119**, 260401 (2017).

[28] P. Prelovšek, Phys. Rev. B **94**, 144204 (2016).

[29] P. Prelovšek, O. S. Barišić, and M. Žnidarič, Phys. Rev. B **94**, 241104(R) (2016).

[30] M. Kozarzewski, P. Prelovšek, and M. Mierzejewski, Phys. Rev. Lett. **120**, 246602 (2018).

[31] M. Środa, P. Prelovšek, and M. Mierzejewski, Phys. Rev. B **99**, 121110(R) (2019).

[32] J. Zakrzewski and D. Delande, Phys. Rev. B **98**, 014203 (2018).

[33] I. V. Protopopov and D. A. Abanin, Phys. Rev. B **99**, 115111 (2019).

[34] G. Lemut, M. Mierzejewski, and J. Bonča, Phys. Rev. Lett. **119**, 246601 (2017).

[35] B. Leipner-Johns and R. Wortis, Phys. Rev. B **100**, 125132 (2019).

[36] C. Hainaut, I. Manai, J.-F. Clément, J. C. Garreau, P. Szriftgiser, G. Lemarié, N. Cherroret, D. Delande, and R. Chicireanu, Nat. Commun. **9**, 1382 (2018).

[37] F. A. An, E. J. Meier, and B. Gadway, Phys. Rev. X **8**, 031045 (2018).

[38] C. Cheng and R. Mondaini, Phys. Rev. A **94**, 053610 (2016).

[39] J. Major, M. Płodzień, O. Dutta, and J. Zakrzewski, Phys. Rev. A **96**, 033620 (2017).

[40] S. D. Geraedts and R. N. Bhatt, Phys. Rev. B **95**, 054303 (2017).

[41] A. Celi, P. Massignan, J. Ruseckas, N. Goldman, I. B. Spielman, G. Juzeliūnas, and M. Lewenstein, Phys. Rev. Lett. **112**, 043001 (2014).

[42] D. Suszalski and J. Zakrzewski, Phys. Rev. A **94**, 033602 (2016).

[43] L. F. Livi, G. Cappellini, M. Diem, L. Franchi, C. Clivati, M. Frittelli, F. Levi, D. Calonico, J. Catani, M. Inguscio, and L. Fallani, Phys. Rev. Lett. **117**, 220401 (2016).

[44] F. H. L. Essler, H. Frahm, F. Göhmann, A. Klümper, and V. E. Korepin, *The One-Dimensional Hubbard Model* (Cambridge University Press, Cambridge, 2016).

[45] S. Zhang, Phys. Rev. Lett. **65**, 120 (1990).

[46] F. Haake, *Quantum Signatures of Chaos* (Springer, Berlin, 2010).

[47] F. Pietracaprina, N. Macé, D. J. Luitz, and F. Alet, SciPost Phys. **5**, 045 (2018).

[48] J. Šuntajs, J. Bonča, T. Prosen, and L. Vidmar, arXiv:1905.06345 [cond-mat.str-el].

[49] D. A. Abanin, J. H. Bardarson, G. D. Tomasi, S. Gopalakrishnan, V. Khemani, S. A. Parameswaran, F. Pollmann, A. C. Potter, M. Serbyn, and R. Vasseur, arXiv:1911.04501 [cond-mat.str-el].

[50] P. Sierant, D. Delande, and J. Zakrzewski, arXiv:1911.06221 [cond-mat.dis-nn].

[51] R. K. Panda, A. Scardicchio, M. Schulz, S. R. Taylor, and M. Žnidarič, Europhys. Lett. **128**, 67003 (2020).

[52] A. Lukin, M. Rispoli, R. Schittko, M. E. Tai, A. M. Kaufman, S. Choi, V. Khemani, J. Léonard, and M. Greiner, Science **364**, 256 (2019).

[53] M. Rispoli, A. Lukin, R. Schittko, S. Kim, M. E. Tai, J. Léonard, and M. Greiner, Nature **573**, 385 (2019).

[54] Y. Y. Atas, E. Bogomolny, O. Giraud, and G. Roux, Phys. Rev. Lett. **110**, 084101 (2013).

[55] S. Nag and A. Garg, Phys. Rev. B **96**, 060203(R) (2017).

[56] S.-H. Lin, B. Sbierski, F. Dorfner, C. Karrasch, and F. Heidrich-Meisner, SciPost Phys. **4**, 002 (2018).

[57] P. Sierant and J. Zakrzewski, New J. Phys. **20**, 043032 (2018).

[58] A. Chandran, C. R. Laumann, and V. Oganesyan, arXiv:1509.04285 [cond-mat.dis-nn].

[59] A. Goremykina, R. Vasseur, and M. Serbyn, Phys. Rev. Lett. **122**, 040601 (2019).

[60] N. Macé, F. Alet, and N. Laflorencie, Phys. Rev. Lett. **123**, 180601 (2019).

[61] I. García-Mata, J. Martin, R. Dubertrand, O. Giraud, B. Georgeot, and G. Lemarié, Phys. Rev. Res. **2**, 012020 (2020).

[62] E. V. H. Doggen, F. Schindler, K. S. Tikhonov, A. D. Mirlin, T. Neupert, D. G. Polyakov, and I. V. Gornyi, Phys. Rev. B **98**, 174202 (2018).

[63] T. Chanda, P. Sierant, and J. Zakrzewski, Phys. Rev. B **101**, 035148 (2020).

[64] D. J. Luitz and Y. B. Lev, Ann. Phys. **529**, 1600350 (2017).

[65] Y. Zhao, S. Ahmed, and J. Sirker, Phys. Rev. B **95**, 235152 (2017).

[66] C. D'Errico, M. Zaccanti, M. Fattori, G. Roati, M. Inguscio, G. Modugno, and A. Simoni, New J. Phys. **9**, 223 (2007).

[67] F. Crépin, N. Laflorencie, G. Roux, and P. Simon, Phys. Rev. B **84**, 054517 (2011).

[68] X. Yu, D. Luo, and B. K. Clark, Phys. Rev. B **98**, 115106 (2018).